

# MULTILEVEL ARTIFICIAL NEURAL NETWORK TRAINING FOR SPATIALLY CORRELATED LEARNING\*

C.B. SCOTT<sup>†</sup> AND ERIC MJOLSNESS<sup>‡</sup>

**Abstract.** Multigrid modeling algorithms are a technique used to accelerate relaxation models running on a hierarchy of similar graphlike structures. We introduce and demonstrate a new method for training neural networks which uses multilevel methods. Using an objective function derived from a graph-distance metric, we perform orthogonally-constrained optimization to find optimal prolongation and restriction maps between graphs. We compare and contrast several methods for performing this numerical optimization, and additionally present some new theoretical results on upper bounds of this type of objective function. Once calculated, these optimal maps between graphs form the core of Multiscale Artificial Neural Network (MsANN) training, a new procedure we present which simultaneously trains a hierarchy of neural network models of varying spatial resolution. Parameter information is passed between members of this hierarchy according to standard coarsening and refinement schedules from the multiscale modelling literature. In our machine learning experiments, these models are able to learn faster than default training, achieving a comparable level of error in an order of magnitude fewer training examples.

**Key words.** Multigrid Methods, Neural Networks, Classification,

**AMS subject classifications.** 46N10, 47N10, 65M55, 68T05, 82C32

**1. Motivation and Background.** Multigrid methods (or multilevel methods when the underlying graph is not a grid) comprise a modeling framework that seeks to ameliorate a core problem in relaxation methods: namely, that these models have differing rates of convergence for fine-scale and coarse-scale modes [29]. Because relaxation methods make updates of a given characteristic length, they are maximally efficient for propagating modes of approximately this wavelength, but ignore finer modes and are inefficient on coarser modes. Multigrid approaches gain computational benefit by addressing these multiple length-scales of behavior using multiple model resolutions, rather than attempting to address them all at the finest scale (in which the coarse modes converge slowly). These methods make use of “prolongation” and “restriction” operators to move between models in a hierarchy of scales. At each level, a “smoothing” step is performed - usually, for multilevel methods a smoothing step consists of one pass of some iterative method for progressing the model at that scale. In this paper, we describe a general algorithm for applying this approach to the training of Artificial Neural Networks (ANNs). In particular, we demonstrate this novel method which combines ideas from machine learning and multilevel modelling by training several hierarchies of Autoencoder networks (ANNs which learn a mapping from data to a lower-dimensional latent space) [9] [4]. By applying multilevel modeling methods we learn this latent representation in far fewer (an order of magnitude) data samples seen by the finest-scale model.

**2. Prior Work.** In this section, we discuss prior attempts to apply ideas from multigrid methods to neural network models. Broadly speaking, prior approaches to

---

\*Submitted to the editors June 14, 2018.

**Funding:** This work was funded by NSF NRT 1633631, and in part by the United States AirForce under Contract No. FA8750-14-C-0011 under the DARPA PPAML program; also by NIH grant R01 HD073179.

<sup>†</sup>Department of Computer Science, University of California, Irvine. ([scottcb@uci.edu](mailto:scottcb@uci.edu)).

<sup>‡</sup>Departments of Computer Science and Mathematics, University of California, Irvine. ([emj@uci.edu](mailto:emj@uci.edu)).

neural net multigrid can be categorized into two classes: (1) Neural network models which are “structurally multigrid”, i.e. are typical neural network models which make use of multiple scales of resolution; and (2) Neural network training processes which are hierarchical in some way, or use a coarsening-refinement procedure as part of the training process. In the first class are approaches such as [8], [24], and [12]. Reference [12] implements a convolutional network in which convolutions make use of a multigrid-like structure similar to a Gaussian pyramid, with the motivation that the network will learn features at multiple scales of resolution. Reference [8] defines a convolution operation, inspired by multigrid methods, that convolves at multiple levels of resolution simultaneously. Reference [24] demonstrates a recurrent neural network model which similarly operates in multiple levels of some scale space; but in this paper the scale space is a space of aggregated language models (specifically, the differing scales are different levels of generality in language models - for example, topic models are coarsest, word models are finest, with document models somewhere in between). Common to all three of these approaches is that they make use of a modified neural net structure while leaving the training process unchanged, except that the network accepts multiresolution inputs.

In contrast, the second class of multilevel neural network models ([23] and [2]) present modified learning procedures which also use methodology similar to multilevel modeling. Reference [2] introduces a network which learns at coarse scales, and then gradually refines its decision making by increasing the resolution of the input space and learning “corrections” at each scale. However, that paper focuses on the capability of a particular family of basis functions for neural networks, and not on the capabilities of the multigrid approach. Reference [23] presents a reframing of the neural network training process as an evolution equation in time, and then applies a method called MGRIT (Multigrid Reduction in Time [7]) to achieve the same results as parallelizing over many runs of training.

Our approach is fundamentally different: we use coarsened versions of the network model to make coarse updates to the weight variables of our model, followed by ‘smoothing steps’ in which the fine-scale weights are refined. This approach is more general than those of [8], [24], and [12], since it can be applied to any feed-forward network and is not tied to a particular network structure. The approach in [23] is to parallelize the training process by reframing it as a continuous-in-time evolution equation, but it still uses the same base model and therefore only learns at one spatial scale. Our method is both structurally multilevel and learns using a multilevel training procedure. Our approach is the first to learn at all spatial scales simultaneously over the course of training, transitioning between neural networks of varying input resolution according to standard multigrid method schedules of coarsening and refinement. To our knowledge, this represents a completely novel approach to combining the powerful data analysis of neural networks with the model acceleration of multiscale modeling.

**3. Theory.** In this section, we first define basic terms used throughout the paper, and explain the core theory of our paper: that of optimal prolongation maps between graph processes and hence graphs. Finally, we discuss numerical methods for finding specific such maps of minimal error, given two input graphs. We will define mathematically what we mean by “error” in Section 3.2.1.

**3.1. Definitions.** In order to describe our objective function, we must first introduce some core concepts related to minimal mapping between graphs.

- Graph Laplacian: We define the Laplacian matrix of a graph  $G$  as  $L(G) =$

$A(G) - D(G)$ , where  $A(G)$  and  $D(G)$  are the adjacency matrix and diagonal degree matrix of the graph, respectively. The eigenvalues of this matrix are referred to as the spectrum of  $G$ . See [3] or [6] for more details on graph Laplacians and spectral graph theory. Our sign convention for  $L$  agrees with the standard continuum Laplacian,  $\Delta$ .

- **Box Product ( $\square$ ) of Graphs:** For  $G_1$  with vertex set  $U = \{u_1, u_2 \dots\}$  and  $G_2$  with vertex set  $V = \{v_1, v_2 \dots\}$ ,  $G_1 \square G_2$  is the graph with vertex set  $U \times V$  and an edge between  $(u_{i_1}, v_{j_1})$  and  $(u_{i_2}, v_{j_2})$  when either of the following is true:
  - $i_1 = i_2$  and  $v_{j_1}$  and  $v_{j_2}$  are adjacent in  $G_2$ , or
  - $j_1 = j_2$  and  $u_{i_1}$  and  $u_{i_2}$  are adjacent in  $G_1$ .
- **Cross Product ( $\times$ ) of Graphs:** For  $G_1$  with vertex set  $U = \{u_1, u_2 \dots\}$  and  $G_2$  with vertex set  $V = \{v_1, v_2 \dots\}$ ,  $G_1 \times G_2$  is the graph with vertex set  $U \times V$  and an edge between  $(u_{i_1}, v_{j_1})$  and  $(u_{i_2}, v_{j_2})$  when both of the following are true:
  - $u_{i_1}$  and  $u_{i_2}$  are adjacent in  $G_1$ , and
  - $v_{j_1}$  and  $v_{j_2}$  are adjacent in  $G_2$ .
- **Prolongation map:** A prolongation map between two graphs  $G_1$  and  $G_2$  of sizes  $n_1$  and  $n_2$ , with  $n_2 \geq n_1$ , is an  $n_2 \times n_1$  matrix of real numbers which is an optimum of the objective function of equation 3.2 below (possibly subject to some set of constraints  $C(P)$ ).
- **Eigenvalue matching:** Given two matrices  $A_1$  and  $A_2$ , and lists of their eigenvalues  $\{\lambda_1^{(1)}, \lambda_2^{(1)}, \dots, \lambda_{n_1}^{(1)}\}$  and  $\{\lambda_1^{(2)}, \lambda_2^{(2)}, \dots, \lambda_{n_2}^{(2)}\}$ , with  $n_2 \geq n_1$ , we define the *minimal eigenvalue matching*  $m^*(A_1, A_2)$  as the matrix  $M$  which minimizes the sum

$$\sum_{i=1}^{n_2} \sum_{j=1}^{n_1} M_{i,j} (\lambda_j^{(1)} - \lambda_i^{(2)})^2$$

subject to the following constraints:

$$(3.1) \quad (M \in \{0, 1\}^{n_2 \times n_1}) \wedge \left( \sum_{i=1}^{n_2} M_{i,j} = 1 \right) \wedge \left( \sum_{j=1}^{n_1} M_{i,j} \leq 1 \right)$$

In the case of eigenvalues with multiplicity  $> 1$ , there may not be one unique such matrix, in which case we distinguish matrices with identical cost by the lexicographical ordering of their occupied indices and take  $m^*(A_1, A_2)$  as the first of those with minimal cost. Additionally, given a way to enumerate these minimal-cost matchings, we can perform combinatorial optimization with respect to some other objective function  $g$ , in order to find optima of  $g(P)$  subject to the constraint that  $P$  is a minimal matching. This matching problem is well-studied and efficient algorithms for solving it exist; we use a Python language implementation [5] of a 1957 algorithm due to Munkres [19].

### 3.2. Optimal Prolongation Maps Between Graphs.

**3.2.1. Our objective function.** Given two graphs  $G_1$  and  $G_2$ , we find the optimal prolongation map between them as follows: We first calculate the graph Laplacians  $L_1$  and  $L_2$ , as well as pairwise vertex Manhattan distance matrices (i.e. the matrix with  $T_{i,j}$  the minimal number of graph edges between vertices  $i$  and  $j$

in the graph),  $T_1$  and  $T_2$ , of each graph. The optimal map is defined as  $P$  which minimizes the matrix function

$$(3.2) \quad \begin{aligned} & \inf_{P|C(P), \alpha>0, \beta>0} E(P) \\ &= \inf_{P|C(P), \alpha>0, \beta>0} \left[ (1-\lambda) \left\| \frac{1}{\sqrt{\alpha}} PL_1 - \sqrt{\alpha} L_2 P \right\|_F \quad \text{“Diffusion Term”} \right. \\ & \quad \left. + \lambda \left\| \frac{1}{\sqrt{\beta}} PT_1 - \sqrt{\beta} T_2 P \right\|_F \right] \quad \text{“Locality Term”}^1 \end{aligned}$$

where  $\|\cdot\|_F$  is the Frobenius norm, and  $C(P)$  is a set of constraints on  $P$  (in particular, we require  $P^T P = I_{n_1}$ , but could also impose other restrictions such as sparsity, regularity, and/or bandedness). The manifold of real-valued orthogonal  $n_2 \times n_1$  matrices with  $n_1 \leq n_2$  is known as the Stiefel manifold; minimization constrained to this manifold is a well-studied problem [22] [26]. This optimization problem can be thought of as measuring the agreement between processes on each graph, as mapped through  $P$ . The expression  $PX_1 - X_2 P$  compares the end result of

1. Advancing process  $X_2$  forward in time and then restricting to the smaller graph, to:
2. Restricting to the smaller graph and then advancing process  $X_1$ .

Parameters  $\alpha$  and  $\beta$  are time rescalings to compensate for different graph sizes; in other words,  $P$  must only ensure that processes 1 and 2 above agree up to some multiplicative time constant. In operator theory terminology, we have a time evolution operator for the single particle diffusion equation:  $L_i^{(R)} = \hat{L}_i^{(R)} - \text{diag}(1 \cdot \hat{L}_i^{(R)})$ . This operator evolves the probability distribution of states of a single-particle diffusion process on a graph  $G_i$  (but other processes could be used - for example, a chemical reaction network or multiple-particle diffusion). The process  $L$  defines a probability-conserving Master Equation of nonequilibrium statistical mechanics  $dp/dt = L \cdot p$  which has formal solution  $p(t) = \exp(tL) \cdot p(0)$ . Pre-multiplication by the prolongation matrix  $P$  is clearly a linear operator i.e. linear transformation from  $\mathbb{R}^{n_1}$  to  $\mathbb{R}^{n_2}$ . Thus, we are requiring  $P$  which minimizes the degree to which the operator diagram

$$\begin{array}{ccc} L_1^{(R)} & \xrightarrow{\Delta t} & L_1^{(R)'} \\ \downarrow P & & \downarrow P \\ L_2^{(R)} & \xrightarrow{\Delta t} & L_2^{(R)'} \end{array} \quad (\text{Diagram 1})$$

fails to commute.  $\Delta t$  of course refers to advancement in time.

We thus include in our objective function terms with 1) graph diffusion and 2) graph locality as the underlying process matrices ( $T$ , the Manhattan distance matrix, cannot be considered a time evolution operator because it is not probability-preserving). Parameter  $\lambda$  adjusts the relative strength of these terms to each other; so we may find “fully diffuse”  $P$  when  $\lambda = 0$  and “fully local”  $P$  when  $\lambda = 1$ . Figure 1 illustrates this tradeoff for an example prolongation problem, including the transition from a global optimum of the diffusion term to a global optimum of the locality

<sup>1</sup>By this we mean the notion that neighborhoods of  $G_1$  should be mapped to neighborhoods of  $G_2$  and vice versa.

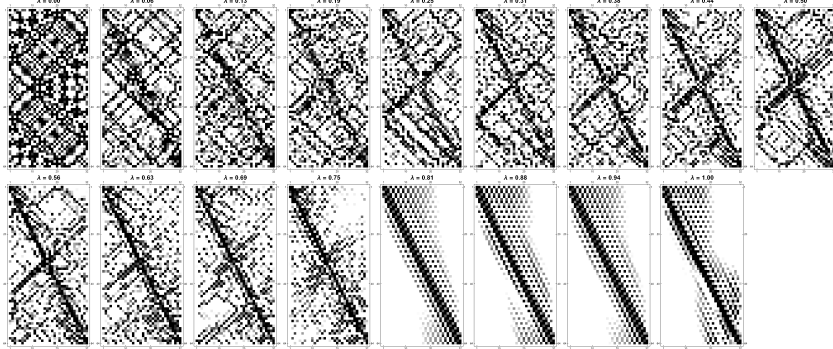


FIG. 1. Several solutions of our objective function found by PyManOpt as  $\lambda$  is tuned from 0 (fully diffuse, top left) to 1 (fully local, bottom right).

term. In each case, we only require  $P$  to map these processes into one another up to a multiplicative constant:  $\alpha$  for the diffusion term and  $\beta$  for the locality term. Exhaustive grid search over  $\alpha$  and  $\beta$  for a variety of prolongations between (a) path graphs and (b) 2D grid graphs of varying sizes has suggested that for prolongation problems where the  $G_i$  are both paths or both grids, the optimal values for these parameters are  $\alpha = 1.0$  and  $\beta = n_1/n_2$ . However, we do not expect this scaling law to hold for general graphs.

### 3.3. Numerical Optimization Results.

**3.3.1. Minimization method.** To find minima of this objective function, we explore several numerical methods. For prototyping, we initially used Nelder-Mead [20] optimization with explicit orthogonality constraints, as implemented in the Mathematica commercial computer algebra program. However, this approach does not scale - in our hands Mathematica was not able to minimize this objective function with more than approximately 200 unknowns in a reasonable amount of time. Our next approach was to use a special-purpose code [28] for orthogonally-constrained gradient descent. While this software package scaled well to pairs of large graphs, it required many random restarts to find minima of our objective function. Motivated by its automatic differentiation capability and its ability to handle larger numbers of unknowns, we tried the TensorFlow minimization package [1]: first custom-written code and then a package called PyManOpt [25] which performs manifold-constrained optimization of arbitrary objective functions expressed as TensorFlow computation graphs. PyManOpt is able to perform first- and second-order minimization while staying within the constraint manifold (rather than our custom code, which takes gradient descent steps and then projects back to the constraint surface). These latter two approaches performed best in terms of optimization solution quality, and we compare them more thoroughly below.

**3.3.2. Initialization.** We initialize our minimization with an upper-bound solution given by the Munkres minimum-cost matching algorithm; the initial  $P$  is  $m^*(L_1, L_2)$  as defined above, i.e. the binary matrix where an entry  $P_{(i,j)}$  is 1 if the pair  $(i,j)$  is one of the minimal-cost pairs selected by the minimum-cost assignment algorithm, and 0 otherwise. While this solution is, strictly speaking, minimizing the error associated with mapping the spectrum of one graph into the spectrum of the other (rather than actually mapping a process running on one graph into a pro-

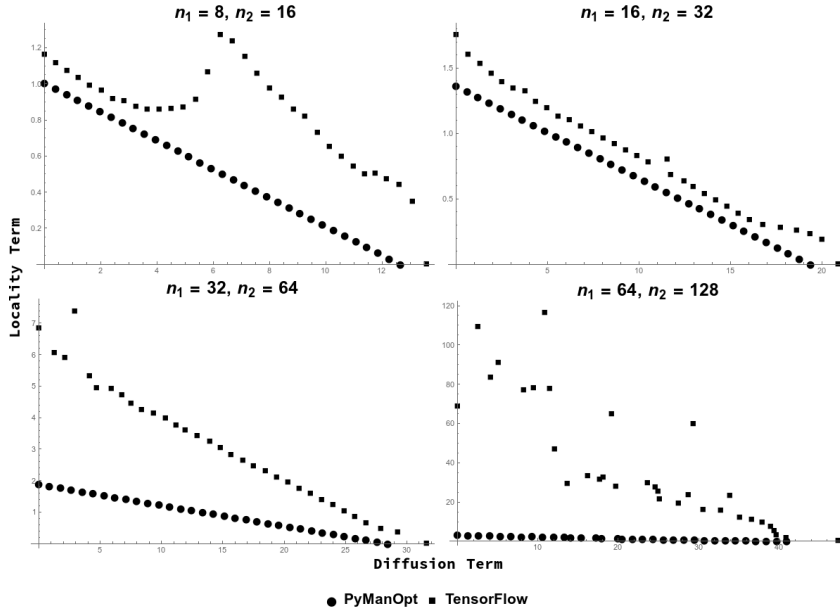


FIG. 2. Tradeoff plot of locality vs. diffusion for several pairs of graphs. Multiple solutions are plotted in each subplot, representing the adjustment of the  $\lambda$  parameter in our objective function from totally local to totally diffuse. We see that the PyManOpt boundary is linear and close to the origin while the TensorFlow boundary is further out and irregular.

cess on the other) we found it to be a reasonable initialization, outperforming both random restarts and initialization with the appropriately sized block matrix  $\begin{pmatrix} I \\ 0 \end{pmatrix}$ . As detailed further in Section 5, the  $P$  found as a solution to this matching problem provides an upper bound for the full orthogonality-constrained optimization problem.

**3.3.3. Comparison of Numerical Methods.** To compare the performance of the TensorFlow method and the PyManOpt method, we explore the performance of both minimization methods as the relative weight  $\lambda$  of the locality and diffusion terms is adjusted. Figure 2 shows the tradeoff plot of the optimized unweighted value of each term as the weight parameter  $\lambda$  is tuned. The four subplots correspond to four runs of this experiment with differing sizes of graphs; in each we find optimal prolongations from a cycle graph of size  $n$  to one of size  $2n$ . The PyManOpt-based minimization code is clearly superior, as we see a clear linear tradeoff between objective function terms as a function of  $\lambda$ . The TensorFlow code which maintains orthogonality by projecting back to the Stiefel manifold falls short of this boundary in all cases. Therefore unless otherwise specified, for the rest of this paper when we discuss solving for  $P$  matrices, we are reporting results of using the PyManOpt method.

**3.3.4. Precomputing  $P$  matrices.** For some structured graph lineages it may be possible to derive formulaic expressions for optimal  $P$  and  $\alpha$ , as a function of the lineage index. For example, during our experiments we discovered species of  $P$  which are local minima of prolongation between path graphs, cycle graphs, and grid graphs. We have additionally derived closed-form expressions for global minima of the diffusion term of our objective function for some graph families (cycle graphs and grid

graphs with periodic boundary conditions). Proof of the optimality of these solutions may be found in the supplementary materials which accompany this paper. However, in practice these global minima are nonlocal (in the sense that they are not close to optimizing the locality term) and thus may not preserve learned spatial rules between weights in levels of our hierarchy. Examples of these formulaic  $P$  matrices can be seen in Figure 3. Each column of that figure shows increasing sizes of  $P$  generated by closed-form solutions which were initially found by solving smaller prolongation problems (for various graph pairs and choices of  $\lambda$ ) and generalizing the solution to higher  $n$ . Many of these examples are similar to what a human being would design as interpolation matrices between cycles and periodic grids. However, (a) they are valid local optima found by our optimization code and (b) our approach generalizes to processes running on more complicated or non-regular graphs, for which there may not be an obvious *a priori* choice of prolongation operator. Out of these multiple species of closed-form solution, those interpolation matrix-like  $P$  seen in the third column of the ‘‘Cycle Graphs’’ section, or sixth column of the ‘‘Grid Graphs’’ section of Figure 3 were the local optima with lowest objective function value (with  $\lambda = 1$ , i.e. they are fully local). As the best optima found by our method(s), these matrices were our choice for line graph and grid graph prolongation operators in our neural network experiments, detailed in Section 4.

Furthermore, given two graph lineages  $G_1^{(1)}, G_1^{(2)}, G_1^{(3)} \dots$  and  $G_1^{(1)}, G_1^{(2)}, G_1^{(3)} \dots$ , and sequences of optimal matrices  $P_1^{(1)}, P_1^{(2)}, P_1^{(3)} \dots$  and  $P_1^{(1)}, P_1^{(2)}, P_1^{(3)} \dots$  mapping between successive members of each, we show in (Section 5.2, Corollary 5.2) conditions under which the value of the objective function at  $P_{\square}^{(i)} = P_1^{(i)} \otimes P_2^{(i)}$  upper bounds the optimal value for prolongations between members of the lineage  $G_1^{(1)} \square G_2^{(1)}, G_1^{(2)} \square G_2^{(2)}, G_1^{(3)} \square G_2^{(3)}, \dots$  (namely, that the two time scaling constants have  $\alpha_1 \approx \alpha_2$ ). We leave open the question of whether such formulaic  $P$  exist for other families of structured graphs (complete graphs,  $k$ -partite graphs, etc.). Even in cases where formulaic  $P$  are not known, the computational cost of numerically optimizing over  $P$  may be amortized, in the sense that once a  $P$ -map is calculated, it may be used in many different hierarchical neural networks or indeed many different multiscale models.

**3.4. Multiscale Artificial Neural Network Algorithm.** In this section we describe the Multiscale Artificial Neural Network (MsANN) training procedure, both in prose and in pseudocode (Algorithm 3.4.2). Let  $\mathcal{M}_0 \dots \mathcal{M}_L$  be a sequence of neural network models with identical ‘‘aspect ratios’’ (meaning the sizes of each layer relative to other layers in the same model) but differing input resolution, so that  $\mathcal{M}_0$  operates at the finest scale and  $\mathcal{M}_L$  at the coarsest. For each model  $\mathcal{M}_l$ , let  $\theta_0^{(l)}, \theta_1^{(l)}, \dots \theta_{n_{\text{vars}}-1}^{(l)}$  be a list of the  $n_{\text{vars}}$  variables (each in matrix or vector form) in some canonical order which is maintained across all scales. Let the symbol  $(P)_j^{(l)}$  represent either:

- If the variables at index  $j$  at levels  $i = 0 \dots L$  are weight matrices between layers  $m_1$  and  $m_2$  of each hierarchy, then  $(P)_j^{(l)}$  represents a pair of matrices  $(P_{\text{input}_j}^{(l)}, P_{\text{output}_j}^{(l)})$ , such that:
  - $P_{\text{input}_j}^{(l)}$  prolongs or restricts between possible values of nodes in layer  $m_1$  of model  $\mathcal{M}_l$ , and values of nodes in layer  $m_1$  of model  $\mathcal{M}_{l+1}$ .
  - $P_{\text{output}_j}^{(l)}$  does the same for possible values of nodes in layer  $m_2$  of each model.
- If the variables at index  $j$  at levels  $i = 0 \dots L$  are bias vectors which are

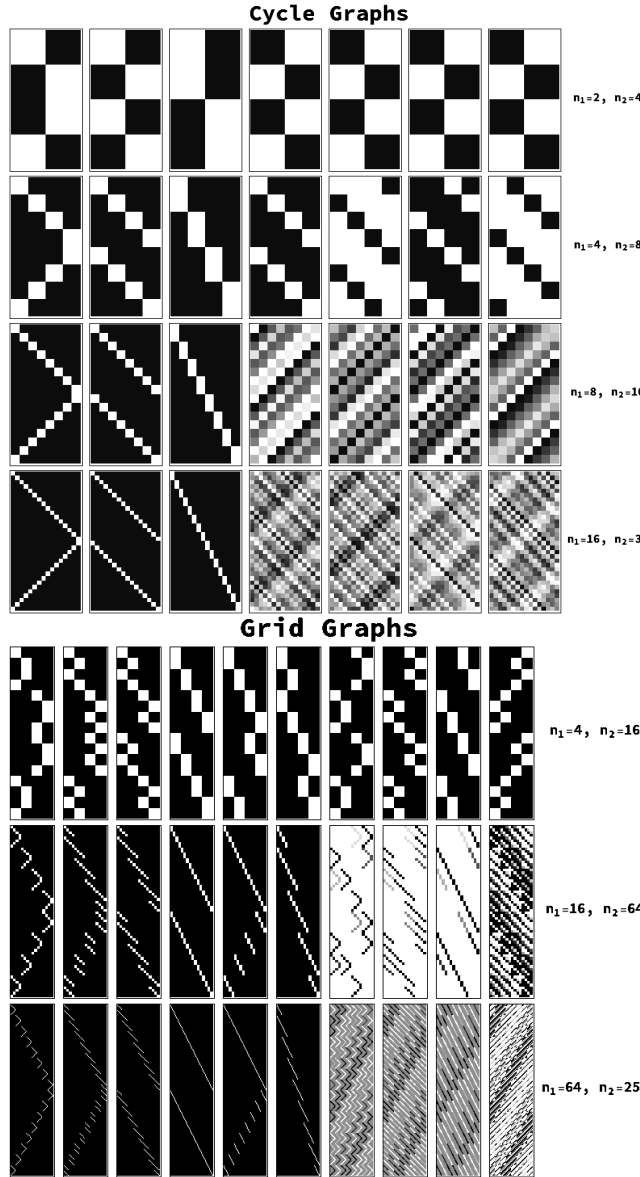


FIG. 3. Examples of  $P$  matrices for cycle graph (top) and grid graph (bottom) prolongation problems of various sizes (given at right), which were generated by a closed-form representation dependent on problem size. Within each of the top and bottom plots, columns represent a series of matrices each generated by a particular numerical recipe, with rows representing increasing sizes of prolongation problem. Each matrix plot is a plot of the absolute value of matrix cell values. These closed-form representations were initially found as local minima of our objective function on small problems and then generalized to closed-form representations. For the “Cycle Graphs” section, columns 1-3 were solutions found with  $\lambda = 1$  (fully local), and the rest were found with  $\lambda = 0$  (fully diffuse). For the “Grid Graphs” section, columns 1-6 are fully local and columns 7-10 are fully diffuse, respectively.

added to layer  $m$  of each hierarchy, then  $(P)_j^{(l)}$  represents a single  $P_j^{(l)}$  which prolongs or restricts between possible values of nodes in layer  $m$  of model  $\mathcal{M}_l$ , and values of nodes in layer  $m$  of model  $\mathcal{M}_{l+1}$ .

As a concrete example, for a hierarchy of single-layer networks  $\mathcal{M}_0, \mathcal{M}_1, \mathcal{M}_2$  each with one weight matrix and one bias vector, we could have  $\theta_0^{(l)} = W^{(l)}, \theta_1^{(l)} = b^{(l)}$  for each  $\mathcal{M}_l$ .  $(P)_0^{(0)}$  would represent a pair of matrices which map between the space of possible values of  $W^{(0)}$  and the space of possible values of  $W^{(1)}$  (in a manner detailed in the next section). On the other hand,  $(P)_1^{(0)}$  would represent a single matrix which maps between  $b^{(0)}$  and  $b^{(1)}$ . Similarly,  $(P)_0^{(1)}$  would map between  $W^{(1)}$  and  $W^{(2)}$ , and  $(P)_1^{(1)}$  between  $b^{(1)}$  and  $b^{(2)}$ . In this section, we describe a general procedure for training such a hierarchy according to standard multilevel modeling schedules of refinement and coarsening, with the result that the finest network, informed by the weights of all coarser networks, requires fewer training examples.

**3.4.1. Weight Prolongation and Restriction Operators.** In this section we introduce the prolongation and restriction operators for neural network weight and bias optimization variables in matrix or vector form respectively.

For a 2D matrix of weights  $W$ , define

$$(3.3) \quad \begin{aligned} \text{Pro}_{(P)} \circ W &\equiv \text{Pro}_{(P_{\text{input}}, P_{\text{output}})} \circ W \equiv P_{\text{input}} W P_{\text{output}}^T \\ \text{Res}_{(P)} \circ W &\equiv \text{Res}_{(P_{\text{input}}, P_{\text{output}})} \circ W \equiv P_{\text{input}}^T W P_{\text{output}} \end{aligned}$$

where  $P_{\text{input}}$  and  $P_{\text{output}}$  are each prolongation maps between graphs which respect the structure of the spaces of inputs and outputs of  $W$ , i.e. whose structure is similar to the structure of correlations in that space. Note that the Pro and Res linear operators satisfy  $\text{Res}_{(P)} \circ \text{Pro}_{(P)} = I$ , the identity operator, so  $\text{Pro}_{(P)} \circ \text{Res}_{(P)}$  is a projection operator. We see in the experiment on mapping MNIST handwritten digits to a latent space (Subsection 4.2), for example, that if the input space has a high degree of two-dimensional correlation between variables, but we use  $P$  calculated between 1D path graphs, our multigrid procedure outlined below will sometimes fail to improve over training at only the finest scale. We hypothesize that this effect may be due to 1D prolongations discarding too much of the 2D correlation in the image data.

For a 1D matrix of biases  $b$ , define

$$(3.4) \quad \begin{aligned} \text{Pro}_{(P)} \circ b &= P \cdot b \\ \text{Res}_{(P)} \circ b &= P^T \cdot b \end{aligned}$$

where as before we require that  $P$  be a prolongation matrix between graphs which are appropriate for the dynamics of the network layer where  $b$  is applied. Again  $\text{Res}_{(P)} \circ \text{Pro}_{(P)} = I$ .

**3.4.2. Multiscale Artificial Neural Network Training.** The Multiscale Artificial Neural Network algorithm is defined in terms of a recursive ‘cycle’ that is analogous to one epoch of default neural network training. Starting with  $\mathcal{M}_0$  (i.e. the finest model in the hierarchy), we call the routine  $\text{MsANN}\text{Cycle}(0)$ , which is defined recursively. At any level  $l$ ,  $\text{MsANN}\text{Cycle}$  trains the network at level  $l$  for  $k$  batches of training examples, recurses by calling  $\text{MsANN}\text{Cycle}(l+1)$ , and then returns to train for  $k$  further batches at level  $l$ . The number of calls to  $\text{MsANN}\text{Cycle}(l+1)$  inside each call to  $\text{MsANN}\text{Cycle}(l)$  is given by a parameter  $\gamma$ . Upon moving from finer to

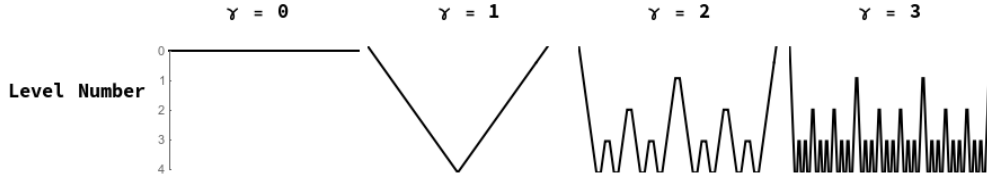


FIG. 4. Visits to models in a hierarchy of neural networks realized by several values of the recursion frequency parameter  $\gamma$ . The  $\gamma = 1$  case and the  $\gamma = 2$  case are referred to as “V-cycles” and “W-cycles”, respectively. Each time the multilevel training procedure visits a level, it performs some number,  $k$ , of smoothing steps (i.e. gradient descent at that resolution) at that model.

coarser scales ( $l \rightarrow l + 1$ ), we compute a ‘residual’: formally, this is the component of the variable orthogonal to that variable’s projection by ( $P$ ) into the coarser space (when a variable is a matrix, we are here referring to orthogonality of the two flattened matrices). We then take the variables at level  $l + 1$  to be coarsened versions of the level  $l$  variables. When moving from coarse to finer scales, we assign to the level  $l$  variables the refinement of the new coarse-state variables, plus the stored residual:

$$\theta_{\text{new}}^{(\text{fine})} = \left( (I - \text{Pro}_{(P)} \circ \text{Res}_{(P)}) \circ \theta_{\text{old}}^{(\text{fine})} \right) + \left( \text{Pro}_{(P)} \circ \theta_{\text{new}}^{(\text{coarse})} \right)$$

This is followed by additional training at the refined scale; this process is normally [27] referred to by the multigrid methods community as ‘restriction’ and ‘prolongation’ followed by ‘smoothing’. The multigrid methods community additionally has special names for this type of recursive refining procedure with  $\gamma = 1$  (“V-Cycles”) and  $\gamma = 2$  (“W-Cycles”). See Figure 4 for an illustration of these contraction and refinement schedules. In our numerical experiments below, we examine the effect of this parameter on multigrid network training.

---

**Algorithm 3.1** One ‘cycle’ of the MsANN procedure.

---

**Procedure** MsANNcycle( $l$ ):

```

    Train model  $\mathcal{M}_l$  for  $k$  batches;
    if max_depth has not been reached then
        for  $1 \leq i \leq \gamma$  do
            for  $0 \leq k \leq n_{\text{vars}} - 1$  do
                Compute and store  $\tilde{\theta}_k^{(l)} = \theta_k^{(l)} - \text{Pro}_{(P)_k^{(l)}} \circ \text{Res}_{(P)_k^{(l)}} \circ \theta_k^{(l)}$ ;
                 $\theta_k^{(l+1)} \leftarrow \text{Res}_{(P)_k^{(l)}} \circ \theta_k^{(l)}$ ;
            end
            MsANNcycle( $l + 1$ );
            for  $0 \leq k \leq n_{\text{vars}} - 1$  do
                 $\theta_k^{(l)} \leftarrow \text{Pro}_{(P)_k^{(l)}}(\theta_k^{(l+1)}) + \tilde{\theta}_k^{(l)}$ ;
            end
        end
    end
    Train model  $\mathcal{M}_l$  for  $k$  batches;

```

---

**4. Machine Learning Experiments.** We present four experiments using this Multiscale Neural Network method. All of the experiments below demonstrate that

our multigrid method outperforms default training (i.e. training only the finest-scale network), in terms of the number of training examples needed to reach a particular mean-squared error (MSE) value. We perform two experiments with synthetic machine vision tasks, as well as two experiments with benchmark image datasets for machine learning. While all of the examples presented here are autoencoder networks (networks whose training task is to reproduce their input at the output layer, while passing through a bottleneck layer or layers), we do not mean to imply that MsANN techniques are constrained to autoencoder networks. All network training uses the standard backpropagation algorithm to compute training gradients, and this is the expected application domain of our method.

**4.1. Simple Machine Vision Task.** As an initial experiment in the capabilities of hierarchical neural networks, we first experiment with autoencoders whose task is to reproduce one or two visual ‘‘objects’’ in a one-dimensional visual field. In both cases, we generate synthetic data by uniformly sampling from

1. The set of binary-valued vectors with one ‘‘object’’ comprising a contiguous set of pixels one-eighth as long as the entire vector set to 1, and the rest zero; and
2. the set of vectors with two such non-overlapping objects.

**4.1.1. Single-Object Autoencoder.** We first test the performance of this procedure on a simple machine vision task. The neural networks in our hierarchy of models each have layer size specification (in number of units)  $[2^n, 2^{n-2}, 2^{n-3}, 2^{n-2}, 2^n]$  for  $n \in \{10, \dots, 6\}$ , with a bias term at each layer and sigmoid logistic activation. At each scale, we present the network with binary vectors which are 0 everywhere except for a contiguous segment of indices of length  $2^{n-3}$  which are set to 1. The objective function to minimize is the MSE between the input and output layers. Each model in the hierarchy is trained using AdamOptimizer in Tensorflow, with learning rate  $\alpha = 0.005$ . Additionally, since the computational complexity of one pass of backpropagation is linear in the number of weights being adjusted, and because level  $l$  of this network has  $8 \times$  more weights than level  $l + 1$ , the number of smoothing steps at each visit to level  $l + 1$  is  $8 \times$  as many smoothing steps as at level  $l$ , to a maximum of 128. The results of this experiment are plotted in Figure 5 and summarized in Table 1. We perform multiple runs of the entire training procedure with differing values of  $k$  (the number of smoothing steps),  $\gamma$  (the multigrid cycle parameter), and  $L$  (depth of hierarchy). Notably, all multigrid schedules demonstrate performance gains over the default network (i.e. the network which trains only at the  $l = 0$  scale), with more improvement for higher values of  $k$ ,  $L$ , and  $\gamma$ . The hierarchy which learned most rapidly was the deepest network with  $k = 1$  and  $\gamma = 3$ . While this approach takes longer in wall-clock time, it achieves similar levels of accuracy as the default model with an order of magnitude fewer samples at the finest-scale model, so it is more statistically efficient.

**4.1.2. Double-Object Autoencoder.** We repeat the above experiment with a slightly more difficult machine vision task - the network must learn to reproduce two (non-overlapping) ‘‘objects’’ in the visual field. We use the same network structure and training procedure, and note that we see again (plotted in Figure 5 and summarized in Table 1) that the hierarchical model is more statistically efficient (in terms of number of samples seen at the finest-scale) in reaching .02 MSE.

**4.2. MNIST.** To supplement the above synthetic experiments with one using real-world data, we perform the same experiment with an autoencoder for the MNIST

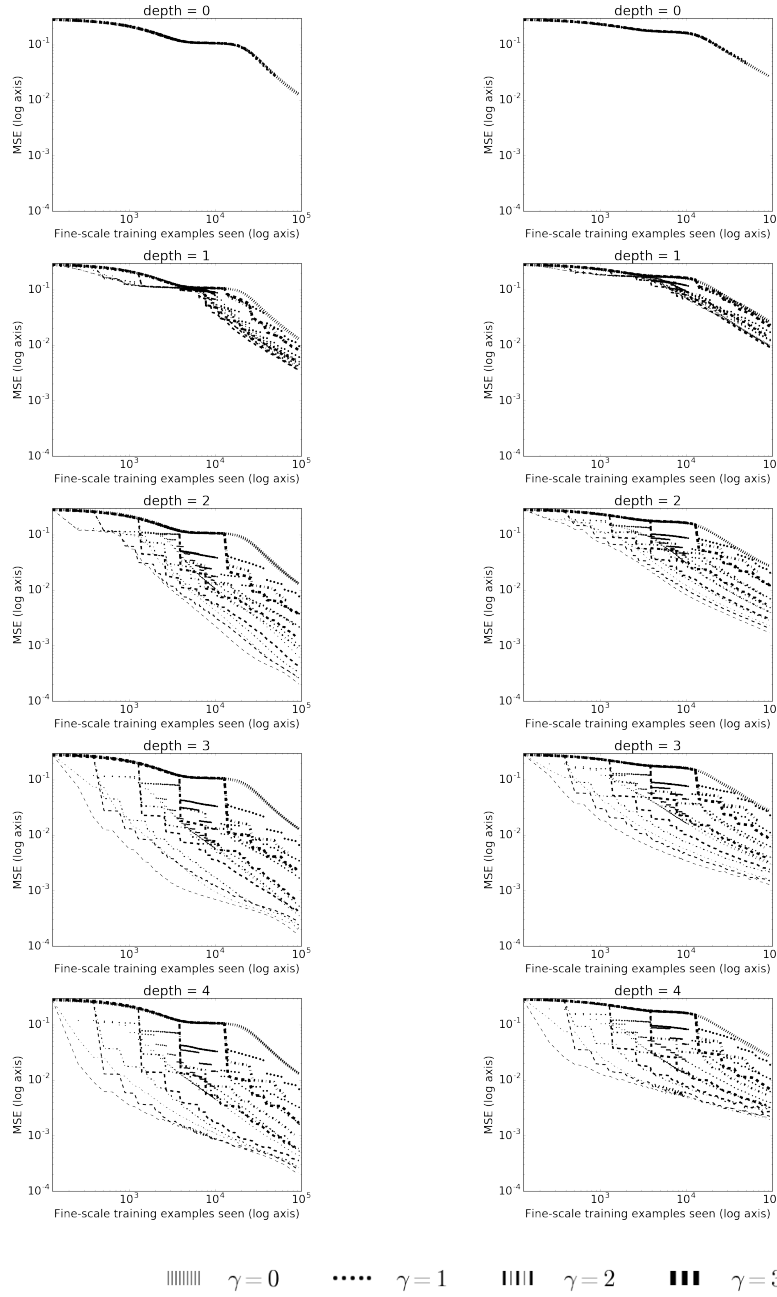


FIG. 5. *Log-log accuracy as a function of fine-scale training examples seen by a variety of hierarchical neural networks training on a simple machine vision task, demonstrating that deeper hierarchies with more multigrid behavior learn more rapidly. Plots are ordered from top to bottom in increasing depth of network hierarchy; left plots are the single object experiments and right plots are the double object experiments. Within each plot, different curves represent different values of the smoothing parameter  $k$  and the recursion parameter  $\gamma$  (see key). Line thickness is proportional to  $\log(k)$ ; line styles represent differing values of  $\gamma$  (see key, above).*

handwritten digit dataset [17] [18]. In this case, rather than the usual MNIST classification task, we use an autoencoder to map the MNIST images into a lower-dimensional space with good reconstruction. As in the 1D vision task, our autoencoder hierarchy has layer specifications dependent on depth: the model at level  $l$  has layer sizes  $[2^{(10-2l)}, 2^{(9-2l)}, 2^{(10-2l)}]$  for  $l$  in  $\{0, 1, 2, 3\}$ . Note here that the input size of each layer decreases by a factor of 4; this is because our dataset consists of two-dimensional images, so halving resolution decreases the number of inputs by a factor of 4. We pre-render four resized versions of the MNIST dataset at image sizes  $32 \times 32$ ,  $16 \times 16$ ,  $8 \times 8$ , and  $4 \times 4$ . As in the 1D vision example, each network in the hierarchy is constructed of fully connected layers with bias terms and sigmoid activation, and smoothing steps are performed with AdamOpt [13] with learning rate 0.005.

In this experiment, we see (in Figure 6 and Table 1) results similar in statistical efficiency improvement to the prior experiment, with one major caveat. In the 1D vision examples, we expect each layer to have spatial correlation similar to the connections in a 1D path graph, and so we use prolongations between path graphs to grow and shrink the layers of the network. However, we found that this approach was ineffective for images, which have strong spatial correlation in two dimensions. This problem was resolved by using, rather than the prolongations between path graphs used above, instead prolongation maps between 2D grid graphs for those layers which we expect to have grid-like spatial correlations (namely, the input and output layers). The difference in performance between these two choices of underlying structure for the prolongation maps can be seen in Figure 6. Indeed, we see similar results to the synthetic data experiment, in that more training steps at the coarser layers results in improved learning performance of the finer networks in the hierarchy.

**4.3. CIFAR10.** As a fourth experiment, we train the same model as subsection 4.2, using the CIFAR-10 [14] dataset - a dataset of natural images of objects (cars, dogs, airplanes). Evaluation curves for learning this dataset can be seen in Figure 7 and are summarized in Table 1. In contrast to the higher quality of performance seen on MNIST (with appropriate choice of  $P$ ) the hierarchy of models is unable to learn to autoencode this dataset efficiently. Both this and the MNIST experiment reach the same final MSE (approximately 0.01). However, that MSE value represents more than a 10x reduction in error for the MNIST dataset. None of the autoencoders tested on CIFAR were able to achieve this proportional reduction in error. This benchmark dataset is complex; most machine learning analyses of it utilize a type of network layer called a Convolution layer [16], which is more efficient at capturing spatial features of images. Therefore, we would expect relatively poor performance of this network architecture. However, the performance of the autoencoder hierarchy still statistically surpasses that of the default network - indicating that our technique is still able to accelerate learning.

**4.4. Summary.** Despite the diversity of these four autoencoder tasks, we uniformly see improvement when models are stacked in the type of multiscale hierarchy we define in equations 3.3 and 3.4. Furthermore, this improvement is marked: the hierarchical models both learn more rapidly than default training and have final error lower than the default model. In many of our test cases, the hierarchical models reached the same level of MSE as the default in an order of magnitude fewer training examples, and continued to improve, surpassing the final level of error reached by the default network.

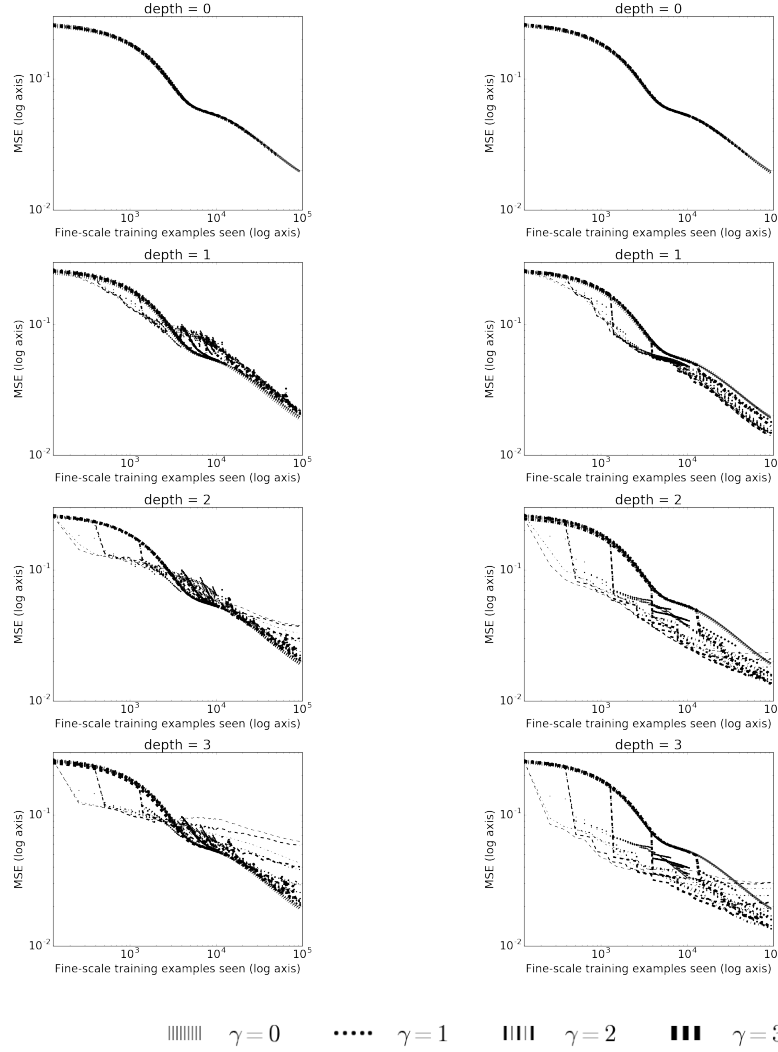


FIG. 6. Log-log plots of mean-squared error (MSE) on MNIST autoencoding task as a function of number of finest-scale training examples seen; the left plots represent multigrid performed with path graph prolongations for each layer while the right plots used grid-based prolongation. While both approaches show gains over default learning, the one which respects the spatial structure of the input data improves more rapidly. Subplot explanations are the same as in Figure 5. Line thickness is proportional to  $\log(k)$ ; line styles represent differing values of  $\gamma$  (see key, above).

**5. Upper Bounds for Diffusion Term.** In this section, we consider two theoretical concerns:

1. Invariance in Frobenius norm of diffusion term solutions under a particular transformation; and
2. Decoupling a prolongation problem between graph products into a sum of prolongation problems of the two sets of graph factors.

We will here rely heavily on properties of the Kronecker product of matrices, as well as the Kronecker sum, which is defined for two matrices  $X \in M_{n \times n}(\mathbb{F})$ ,  $Y \in M_{m \times m}(\mathbb{F})$

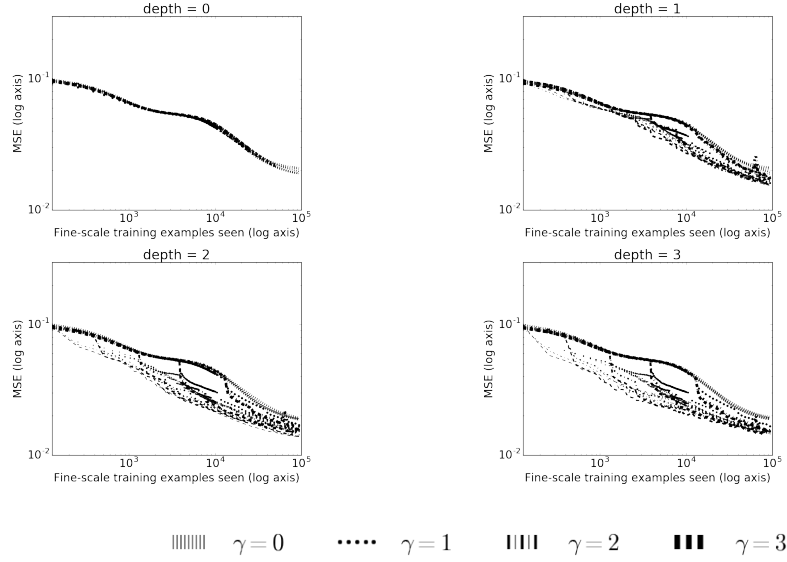


FIG. 7. *Log-log accuracy as a function of fine-scale training examples seen by a variety of hierarchical neural networks training on a complex image recognition task, demonstrating that (a) flat autoencoder networks are unable to optimally learn this dataset even with hierarchical assistance, though (b) MsANN training still accelerates the best available result. Subplot explanations are the same as in Figure 5. Line thickness is proportional to  $\log(k)$ ; line styles represent differing values of  $\gamma$  (see key, above).*

as follows:

$$X \oplus Y = X \otimes I_m + I_n \otimes Y$$

where  $\otimes$  is the Kronecker or outer product of two matrices ([10], Section 11.4).

**5.1. Invariance of objective function evaluation of  $P$  under eigenspace transformation.** For the purpose of the calculations in this section, we restrict ourselves to the “diffusion” term of our objective function 3.2 (the term which coerces two diffusion processes to agree), which we will write as

$$(5.1) \quad D_{P,\alpha}(G_1, G_2) = \left\| \frac{1}{\sqrt{\alpha}} PL_1 - \sqrt{\alpha} L_2 P \right\|_F.$$

Because  $L_1$  and  $L_2$  are each real and symmetric, they may both be diagonalized as  $L_i = U_i \Lambda_i U_i^T$  where  $U_i$  is a rotation matrix and  $\Lambda_i$  is a diagonal matrix with the eigenvalues of  $L_i$  on the diagonal. Substituting into 5.1, we have

$$\begin{aligned} D_{P,\alpha}(G_1, G_2) &= \left\| \frac{1}{\sqrt{\alpha}} PL_1 - \sqrt{\alpha} L_2 P \right\|_F \\ &= \left\| \frac{1}{\sqrt{\alpha}} PU_1 \Lambda_1 U_1^T - \sqrt{\alpha} U_2 \Lambda_2 U_2^T P \right\|_F \\ &= \left\| \frac{1}{\sqrt{\alpha}} (U_2^T P U_1) \Lambda_1 - \sqrt{\alpha} \Lambda_2 (U_2^T P U_1) \right\|_F \\ &= \left\| \frac{1}{\sqrt{\alpha}} \tilde{P} \Lambda_1 - \sqrt{\alpha} \Lambda_2 \tilde{P} \right\|_F \end{aligned}$$

TABLE 1

Best performance in each Multiscale ANN experiment for a variety of metrics, with associated values of hyperparameters  $d$  (depth of hierarchy),  $k$  (number of smoothing steps), and  $\gamma$  (multigrid recursion parameter). Entries marked with (default training) had either  $\gamma = 0$  or  $d = 0$  and so were functionally identical to default training.

Metric	Value	Default	Multigrid Parameters
One-object vision task:			
Worst final MSE	0.082620	<b>0.012577</b>	(default training)
Best final MSE	<b>0.000195</b>	0.012577	$\gamma = 2$ , depth = 3, $k = 1$
Min log-log slope during training	<b>-66.474084</b>	-1.590372	$\gamma = 3$ , depth = 4, $k = 30$
Fine-scale examples needed to decrease initial MSE by 10x	<b>256</b>	48256	$\gamma = 3$ , depth = 4, $k = 1$
Two-object vision task:			
Worst final MSE	0.097007	<b>0.026754</b>	(default training)
Best final MSE	<b>0.001256</b>	0.026754	$\gamma = 3$ , depth = 3, $k = 1$
Min log-log slope during training	<b>-55.927604</b>	-1.103932	$\gamma = 3$ , depth = 4, $k = 30$
Fine-scale examples needed to decrease initial MSE by 10x	<b>384</b>	93952	$\gamma = 3$ , depth = 4, $k = 1$
MNIST Dataset:			
Worst final MSE	0.039343	<b>0.019809</b>	(default training)
Best final MSE	<b>0.013498</b>	0.019809	$\gamma = 3$ , depth = 2, $k = 100$
Min log-log slope during training	<b>-23.211566</b>	-0.850736	$\gamma = 3$ , depth = 3, $k = 30$
Fine-scale examples needed to decrease initial MSE by 10x	<b>9472</b>	58368	$\gamma = 3$ , depth = 2, $k = 10$
CIFAR Dataset:			
Worst final MSE	0.029462	<b>0.019506</b>	(default training)
Best final MSE	<b>0.013701</b>	0.019506	$\gamma = 2$ , depth = 2, $k = 1$
Min log-log slope during training	<b>-12.525581</b>	-0.526287	$\gamma = 3$ , depth = 3, $k = 30$
Fine-scale examples needed to decrease initial MSE by 10x	N/A	N/A	N/A

where  $\tilde{P} = U_2^T P U_1$  is and orthogonal matrix  $\tilde{P}^T \tilde{P} = I$  if and only if  $P$  is. Since the Frobenius norm is invariant under multiplication by rotation matrices, this is a reformulation of our original Laplacian matrix objective function in terms of the spectra of the two graphs. Optimization of this modified form of the objective function subject to orthogonality constraints on  $P$  is upper-bounded by optimization over matchings of eigenvalues: for any fixed  $\alpha$  the eigenvalue matching problem has the same objective function, but our optimization is over all real valued orthogonal  $P$ . The orthogonality constraint is a relaxed version of the constraints on matching problems (Equation 3.1) discussed in subsection 3.1, since matching matrices  $M$  are also orthogonal ( $M^T M = I$ ). Many algorithms exist for solving the inner partial and 0-1 constrained minimum-cost assignment problems, such as the Munkres algorithm (also in subsection 3.1).

We note three corollaries of the above argument:

1. Optimal or near-optimal  $\tilde{P}$  in eigenvalue-space maintain their optimality through the mapping  $U_2 \cdot U_1^T$  back to graph-space.
2. Solutions which are within  $\epsilon$  of the optimum in  $\tilde{P}$ -space are also within  $\epsilon$  of the optimum in  $P$ -space; and
3. More precisely, if they exist, zero-cost eigenvalue matchings correspond exactly with zero-cost  $P$ .

A natural next question would be why it might be worthwhile to work in the original graph-space, rather than always optimizing this simpler eigenvalue-matching problem instead. In many cases (path graphs, cycle graphs) the spectrum of a member  $G_l$  of a graph lineage is a subset of that of  $G_{l+1}$ , guaranteeing that zero-cost eigenvalue matchings (and thus, by the argument above, prolongations with zero diffusion cost) exist. However, when this is not the case, the above argument only upper bounds the true distance, since the matching problem constraints are more strict. Thus, numerical optimization over  $P$ , with orthogonality constraints only, may find a better bound on  $D^{P,\alpha}(G_l, G_{l+1})$ .

**5.2. Decomposing Graph Product Prolongations.** We next consider the problem of finding optimal prolongations between two graphs  $\mathbf{G}_{\square}^{(1)} = G_1^{(1)} \square G_1^{(2)}$  and  $\mathbf{G}_{\square}^{(2)} = G_2^{(1)} \square G_2^{(2)}$  when optimal prolongations are known between  $G_1^{(1)}$  and  $G_2^{(1)}$ , and  $G_1^{(2)}$  and  $G_2^{(2)}$ . We show that under some reasonable assumptions, these two prolongation optimizations decouple - we may thus solve them separately and combine the solutions to obtain the optimal prolongations between the two product graphs.

For the graph box product, we have trivially

$$\begin{aligned}
L_{\square}^{(j)} &= L(G_1^{(j)} \square G_2^{(j)}) \\
&= A(G_1^{(j)} \square G_2^{(j)}) - D(G_1^{(j)} \square G_2^{(j)}) \\
&= \left( A(G_1^{(j)}) \otimes I_2^{(j)} + I_1^{(j)} \otimes A(G_2^{(j)}) \right) - \left( D(G_1^{(j)}) \otimes I_2^{(j)} + I_1^{(j)} \otimes D(G_2^{(j)}) \right) \\
&= \left( A(G_1^{(j)}) \otimes I_2^{(j)} - D(G_1^{(j)}) \otimes I_2^{(j)} \right) - \left( I_1^{(j)} \otimes A(G_2^{(j)}) - I_1^{(j)} \otimes D(G_2^{(j)}) \right) \\
&= (L_1^{(j)} \otimes I_2^{(j)}) + (I_1^{(j)} \otimes L_2^{(j)}) \\
&= L(G_1^{(j)}) \oplus L(G_2^{(j)})
\end{aligned}$$

where  $\oplus$  is the Kronecker sum of matrices as previously defined. We calculate

$$\begin{aligned}
D^{P,\alpha} \left( G_{\square}^{(1)}, G_{\square}^{(2)} \right) &= \left\| \frac{1}{\sqrt{\alpha}} PL_{\square}^{(1)} - \sqrt{\alpha} L_{\square}^{(2)} P \right\|_F \\
&= \left\| \frac{1}{\sqrt{\alpha}} P \left( (L_1^{(1)} \otimes I_2^{(1)}) + (I_1^{(1)} \otimes L_2^{(1)}) \right) \right. \\
&\quad \left. - \sqrt{\alpha} \left( (L_1^{(2)} \otimes I_2^{(2)}) + (I_1^{(2)} \otimes L_2^{(2)}) \right) P \right\|_F \\
&= \left\| \left( \frac{1}{\sqrt{\alpha}} P (L_1^{(1)} \otimes I_2^{(1)}) - \sqrt{\alpha} (L_1^{(2)} \otimes I_2^{(2)}) P \right) \right. \\
&\quad \left. + \left( \frac{1}{\sqrt{\alpha}} P (I_1^{(1)} \otimes L_2^{(1)}) - \sqrt{\alpha} (I_1^{(2)} \otimes L_2^{(2)}) P \right) \right\|_F
\end{aligned}$$

Now we try out the assumption that  $P = P_1 \otimes P_2$ , which restricts the search space over  $P$  and may increase the objective function:

$$\begin{aligned}
D^{P,\alpha} \left( G_{\square}^{(1)}, G_{\square}^{(2)} \right) &= \left\| \left[ \frac{1}{\sqrt{\alpha}} (P_1 \otimes P_2) (L_1^{(1)} \otimes I_2^{(1)}) \right. \right. \\
&\quad \left. \left. - \sqrt{\alpha} (L_1^{(2)} \otimes I_2^{(2)}) (P_1 \otimes P_2) \right] \right. \\
&\quad \left. + \left[ \frac{1}{\sqrt{\alpha}} (P_1 \otimes P_2) (I_1^{(1)} \otimes L_2^{(1)}) \right. \right. \\
&\quad \left. \left. - \sqrt{\alpha} (I_1^{(2)} \otimes L_2^{(2)}) (P_1 \otimes P_2) \right] \right\|_F \\
&= \left\| \left( \frac{1}{\sqrt{\alpha}} (P_1 L_1^{(1)} \otimes P_2) - \sqrt{\alpha} (L_1^{(2)} P_1 \otimes P_2) \right) \right. \\
&\quad \left. + \left( \frac{1}{\sqrt{\alpha}} (P_1 \otimes P_2 L_2^{(1)}) - \sqrt{\alpha} (P_1 \otimes L_2^{(2)} P_2) \right) \right\|_F \\
&= \left\| \left( \left( \frac{1}{\sqrt{\alpha}} P_1 L_1^{(1)} - \sqrt{\alpha} L_1^{(2)} P_1 \right) \otimes P_2 \right) \right\|_F
\end{aligned}$$

$$+ \left\| \left( P_1 \otimes \left( \frac{1}{\sqrt{\alpha}} P_2 L_2^{(1)} - \sqrt{\alpha} L_2^{(2)} P_2 \right) \right) \right\|_F$$

Since  $\|A + B\|_F \leq \|A\|_F + \|B\|_F$ ,

$$\begin{aligned} &\leq \left\| \left( \left( \frac{1}{\sqrt{\alpha}} P_1 L_1^{(1)} - \sqrt{\alpha} L_1^{(2)} P_1 \right) \otimes P_2 \right) \right\|_F \\ &\quad + \left\| \left( P_1 \otimes \left( \frac{1}{\sqrt{\alpha}} P_2 L_2^{(1)} - \sqrt{\alpha} L_2^{(2)} P_2 \right) \right) \right\|_F \\ &= \left\| \frac{1}{\sqrt{\alpha}} P_1 L_1^{(1)} - \sqrt{\alpha} L_1^{(2)} P_1 \right\|_F \|P_2\|_F \\ &\quad + \|P_1\|_F \left\| \frac{1}{\sqrt{\alpha}} P_2 L_2^{(1)} - \sqrt{\alpha} L_2^{(2)} P_2 \right\|_F, \end{aligned}$$

Thus assuming  $P = P_1 \otimes P_2$

$$\begin{aligned} D^{P,\alpha} \left( G_{\square}^{(1)}, G_{\square}^{(2)} \right) &\leq \left\| \tilde{P}_2 \right\|_F D_{\alpha, P_1} \left( G_1^{(1)}, G_1^{(2)} \right) \\ &\quad + \left\| \tilde{P}_1 \right\|_F D_{\alpha, P_2} \left( G_2^{(1)}, G_2^{(2)} \right), \end{aligned}$$

which is a weighted sum of objectives of the optimizations for prolongation from  $G_1^{(1)}$  to  $G_1^{(2)}$  and  $G_2^{(1)}$  to  $G_2^{(2)}$ . Recall that our original constraint on  $P$ , was that  $P^T P = I$ ; since  $P = P_1 \otimes P_2$  this is equivalent (by a property of the Kronecker product; see Corollary 13.8 in [15]) to the coupled constraints on  $P_1$  and  $P_2$ :

$$(5.2) \quad \left( P_1^T P_1 = \frac{1}{\eta} I_1^{(1)} \right) \quad \wedge \quad \left( P_2^T P_2 = \eta I_2^{(1)} \right)$$

for some  $\eta \in \mathbb{R}$ . For any  $P_1, P_2$  which obey 5.2, we may rescale them by  $\eta$  to make them orthogonal without changing the value of the objective, so we take  $\eta = 1$  in subsequent calculations. Noting that  $\|A\|_F = \sqrt{\text{Tr}(A^T A)}$ , we see that

$$\|P_1\|_F = \sqrt{\text{Tr}(I_1^{(1)})} = \sqrt{n_1^{(1)}} \quad \text{and similarly} \quad \|P_2\|_F = \sqrt{n_2^{(1)}}.$$

Thus, we have proven the following:

**THEOREM 5.1.** *Assuming that  $P$  decomposes as  $P = P_1 \otimes P_2$ , the diffusion distance  $D_{P,\alpha} \left( G_{\square}^{(1)}, G_{\square}^{(2)} \right)$  between  $G_{\square}^{(1)}$  and  $G_{\square}^{(2)}$  is bounded above by the strictly monotonically increasing function of the two distances  $D_{P_1,\alpha}$  and  $D_{P_2,\alpha}$ :*

$$\mathcal{F}(D_{P_1,\alpha}, D_{P_2,\alpha}) = \sqrt{n_2^{(1)}} D_{P_1,\alpha} + \sqrt{n_1^{(1)}} D_{P_2,\alpha},$$

*Namely,*

$$D_{P,\alpha} \left( G_{\square}^{(1)}, G_{\square}^{(2)} \right) \leq \mathcal{F} \left( D_{P_1,\alpha} \left( G_1^{(1)}, G_1^{(2)} \right), D_{P_2,\alpha} \left( G_2^{(1)}, G_2^{(2)} \right) \right)$$

Thus, the original optimization over the product graphs decouples into separate optimizations over the two sets of factors, constrained to have the same value of  $\alpha$ . Additionally, since the requirement that  $P = P_1 \otimes P_2$  is an additional constraint,

**COROLLARY 5.2.** *If  $(\alpha_1, P_1)$  and  $(\alpha_2, P_2)$ , subject to orthogonality constraints, are optima of  $D_{\alpha, P}(G_1^{(1)}, G_1^{(1)})$  and  $D_{\alpha, P}(G_2^{(1)}, G_2^{(1)})$ , and furthermore if  $\alpha_1 = \alpha_2$ , then the value of  $D_{P, \alpha}(G_1^{(1)} \square G_2^{(1)}, G_1^{(2)} \square G_2^{(2)})$  for an optimal  $P$  is upper bounded by  $D_{P_1 \otimes P_2, \alpha_1}(G_1^{(1)} \square G_2^{(1)}, G_1^{(2)} \square G_2^{(2)})$ .*

This upper bound on the original objective function is a monotonically increasing function of the objectives for the two smaller problems. A consequence of this upper bound is that if  $D_{P_1, \alpha}(G_1^{(1)}, G_1^{(2)}) \leq \epsilon_1$  and  $D_{P_2, \alpha}(G_2^{(1)}, G_2^{(2)}) \leq \epsilon_2$ , then the composite solution  $P_1 \otimes P_2$  must have  $D_{P_1 \otimes P_2, \alpha}(G_1^{(1)}, G_1^{(2)}) \leq \epsilon = (\sqrt{\epsilon_1} + \sqrt{\epsilon_2}) \max(\epsilon_1, \epsilon_2)$  - so if both of these distances are arbitrarily small then the composite distance must also be small. Furthermore, if only one of these is small, so that  $D_{P_1, \alpha}(G_1^{(1)}, G_1^{(2)}) \approx 0$  or  $D_{P_2, \alpha}(G_2^{(1)}, G_2^{(2)}) \approx 0$ , then  $D_{P_1 \otimes P_2, \alpha} \approx D_{P_2, \alpha}$  or  $D_{P_1 \otimes P_2, \alpha} \approx D_{P_1, \alpha}$ , respectively.

We have experimentally found that many families of graphs do not require scaling between the two diffusion processes: the optimal  $(\alpha, P)$  pair has  $\alpha = 1$ . In particular, prolongation between path (cycle) graphs of size  $n$  and size  $2n$  always have  $\alpha_{\text{optimal}} = 1$ , since the spectrum of the former graph is a subset of that of the larger - therefore, there is a matching solution of cost 0 which by the argument above can be mapped to a graph-space  $P$  with objective function value 0 (we prove this in Section ?? of the Supplementary Material to this paper). In this case, the two terms of the upper bound are totally decoupled and may each be optimized separately (whereas in the form given above, they both depend on a  $\alpha$ ).

**6. Conclusion and Future Work.** We have introduced a novel method for multiscale modeling, which relies on a novel prolongation and restriction operator to move between models in a hierarchy. These prolongation and restriction operators are the optima of an objective function we introduce which is a natural distance metric on graphs and graph lineages. We prove several important properties of this objective function, including an upper bound which allows us to decouple a difficult optimization into two smaller optimization problems under certain circumstances.

Additionally, we demonstrate an algorithm which makes use of these operators to simultaneously train models in a hierarchy of neural networks (specifically, autoencoder neural networks). This Multiscale Artificial Neural Network (MsANN) approach statistically outperforms training only at the finest scale, achieving lower error than the default model and also reaching the default model's best performance in an order of magnitude fewer training examples. Future work will focus on investigating the properties of the distance metric on graphs defined by our objective function, as well as modifying the MsANN algorithm to perform the same type of hierarchical learning on more complicated ANN models, such as Convolutional Neural Networks (CNNs), as well as non-autoencoding tasks, e.g. classification.

**Acknowledgments.** This work was supported by the National Science Foundation NRT Award number 1633631, and also in part by the United States Air Force under Contract No. FA8750-14-C-0011 under the DARPA PPAML program; also by NIH grant R01 HD073179, and by the Leverhulme Trust, and by the hospitality of the Sainsbury Laboratory Cambridge University.

## REFERENCES

- [1] M. ABADI, P. BARHAM, J. CHEN, Z. CHEN, A. DAVIS, J. DEAN, M. DEVIN, S. GHEMAWAT, G. IRVING, M. ISARD, ET AL., *Tensorflow: A System for Large-Scale Machine Learning.*, in OSDI, vol. 16, 2016, pp. 265–283.
- [2] B. R. BAKSHI AND G. STEPHANOPOULOS, *Wave-Net: A Multiresolution, Hierarchical Neural Network with Localized Learning*, AIChE Journal, 39 (1993), pp. 57–81.
- [3] M. BELKIN AND P. NIYOGI, *Laplacian Eigenmaps and Spectral Techniques for Embedding and Clustering*, in Advances in Neural Information Processing Systems, 2002, pp. 585–591.
- [4] H. BOURLARD AND Y. KAMP, *Auto-Association by Multilayer Perceptrons and Singular Value Decomposition*, Biological Cybernetics, 59 (1988), pp. 291–294.
- [5] B. M. CLAPPER, *Munkres Implementation for Python*, 2008–, <http://software.clapper.org/munkres/>. [Online; accessed June 10, 2018].
- [6] D. M. CVETKOVIC, P. ROWLINSON, AND S. SIMIC, *An Introduction to the Theory of Graph Spectra*, Cambridge University Press Cambridge, UK, 2010.
- [7] R. D. FALGOUT, S. FRIEDHOFF, T. V. KOLEV, S. P. MACLACHLAN, AND J. B. SCHRODER, *Parallel Time Integration with Multigrid*, SIAM Journal on Scientific Computing, 36 (2014), pp. C635–C661.
- [8] E. M. GRAIS, H. WIERSTORF, D. WARD, AND M. D. PLUMBLEY, *Multi-Resolution Fully Convolutional Neural Networks for Monaural Audio Source Separation*, arXiv preprint arXiv:1710.11473, (2017).
- [9] G. E. HINTON AND R. R. SALAKHUTDINOV, *Reducing the Dimensionality of Data with Neural Networks*, Science, 313 (2006), pp. 504–507.
- [10] L. HOGBEN, *Handbook of Linear Algebra*, CRC Press, 2006.
- [11] E. JONES, T. OLIPHANT, P. PETERSON, ET AL., *SciPy: Open Source Scientific Tools for Python*, 2001–, <http://www.scipy.org/>. [Online; accessed June 10, 2018].
- [12] T.-W. KE, M. MAIRE, AND S. X. YU, *Neural Multigrid*, arXiv preprint arXiv:1611.07661, (2016).
- [13] D. P. KINGMA AND J. BA, *Adam: A Method for Stochastic Optimization*, arXiv preprint arXiv:1412.6980, (2014).
- [14] A. KRIZHEVSKY, V. NAIR, AND G. HINTON, *The CIFAR-10 Dataset*, online: <http://www.cs.toronto.edu/kriz/cifar.html>, (2014). [Accessed June 10, 2018].
- [15] A. J. LAUB, *Matrix Analysis for Scientists and Engineers*, vol. 91, SIAM, 2005.
- [16] Y. LECUN, Y. BENGIO, AND G. HINTON, *Deep Learning*, Nature, 521 (2015), p. 436.
- [17] Y. LECUN, L. BOTTOU, Y. BENGIO, AND P. HAFFNER, *Gradient-Based Learning Applied to Document Recognition*, Proceedings of the IEEE, 86 (1998), pp. 2278–2324.
- [18] Y. LECUN, C. CORTES, AND C. BURGES, *MNIST Handwritten Digit Database*, AT&T Labs [Online]. Available: <http://yann.lecun.com/exdb/mnist>, 2 (2010). [Accessed June 10, 2018].
- [19] J. MUNKRES, *Algorithms for the Assignment and Transportation Problems*, Journal of the Society for Industrial and Applied Mathematics, 5 (1957), pp. 32–38.
- [20] J. A. NELDER AND R. MEAD, *A Simplex Method for Function Minimization*, The Computer Journal, 7 (1965), pp. 308–313.
- [21] T. OLIPHANT, *A Guide to NumPy*, 2006.
- [22] T. RAPCSÁK, *On Minimization on Stiefel Manifolds*, European Journal of Operational Research, 143 (2002), pp. 365–376.
- [23] J. B. SCHRODER, *Parallelizing Over Artificial Neural Network Training Runs with Multigrid*, arXiv preprint arXiv:1708.02276, (2017).
- [24] I. V. SERBAN, T. KLINGER, G. TESAURO, K. TALAMADUPULA, B. ZHOU, Y. BENGIO, AND A. C. COURVILLE, *Multiresolution Recurrent Neural Networks: An Application to Dialogue Response Generation*, in AAAI, 2017, pp. 3288–3294.
- [25] J. TOWNSEND, N. KOEP, AND S. WEICHWALD, *Pymanopt: A Python Toolbox for Optimization on Manifolds using Automatic Differentiation*, arXiv preprint arXiv:1603.03236, (2016).
- [26] P. TURAGA, A. VEERARAGHAVAN, AND R. CHELLAPPA, *Statistical Analysis on Stiefel and Grassmann Manifolds with Applications in Computer Vision*, in Computer Vision and Pattern Recognition, 2008. CVPR 2008. IEEE Conference on, IEEE, 2008, pp. 1–8.
- [27] P. VANĚK, J. MANDEL, AND M. BREZINA, *Algebraic Multigrid by Smoothed Aggregation for Second and Fourth Order Elliptic Problems*, Computing, 56 (1996), pp. 179–196.
- [28] Z. WEN AND W. YIN, *A Feasible Method for Optimization with Orthogonality Constraints*, Mathematical Programming, 142 (2013), pp. 397–434.
- [29] H. YSERENTANT, *Old and New Convergence Proofs for Multigrid Methods*, Acta Numerica, 2 (1993), pp. 285–326.